

The Role of Ice–Ocean Interactions in the Variability of the North Atlantic Thermohaline Circulation

MARIKA M. HOLLAND,* CECILIA M. BITZ, MICHAEL EBY, AND ANDREW J. WEAVER

School of Earth and Ocean Sciences, University of Victoria, Victoria, British Columbia, Canada

(Manuscript received 6 July 1999, in final form 2 April 2000)

ABSTRACT

The simulated influence of Arctic sea ice on the variability of the North Atlantic climate is discussed in the context of a global coupled ice–ocean–atmosphere model. This coupled system incorporates a general circulation ocean model, an atmospheric energy moisture balance model, and a dynamic–thermodynamic sea ice model. Under steady seasonal forcing, an equilibrium solution is obtained with very little variability. To induce variability in the model, daily varying stochastic anomalies are applied to the wind forcing of the Northern Hemisphere sea ice cover. These stochastic anomalies have observed spatial patterns but are random in time. Model simulations are run for 1000 yr from an equilibrium state and the variability in the system is analyzed. The sensitivity of the system to the ice–ocean coupling of both heat and freshwater is also examined.

Under the stochastic forcing conditions, the thermohaline circulation (THC) responds with variability that is approximately 10% of the mean. This variability has enhanced spectral power at interdecadal timescales that is concentrated at approximately 20 yr. It is forced by fluctuations in the export of ice from the Arctic into the North Atlantic. Substantial changes in sea surface temperature and salinity are related to changes in the overturning circulation and the sea ice coverage in the northern North Atlantic. Additionally, the THC variability influences the Arctic Basin through heat transport under the ice pack.

Results from sensitivity studies suggest that the freshwater exchange from the variable ice cover is the dominant process for forcing variability in the overturning. The simulated Arctic ice export appears to provide stochastic forcing to the northern North Atlantic that excites a damped oscillatory ocean-only mode. The insulating capacity of the variable sea ice has a negligible effect on the THC. Ice–ocean thermal coupling acts to damp THC variability, causing an approximately 25% reduction in the THC standard deviation.

1. Introduction

Interdecadal climate variability is a subject of growing interest. Anthropogenic effects on climate change may be masked by the natural variability of the system. An understanding of this inherent variability is essential if we are to determine the influence that we are having on the natural environment.

The thermohaline circulation (THC) is an important regulator of the meridional heat transport in the North Atlantic and is largely responsible for the relatively warm climates of northern Europe [see Weaver et al. (1999) for a review]. Paleoclimate studies suggest the possible importance of the THC for climate variability on a large range of timescales, from the millennial changes involved in the Younger Dryas event (Broecker et al.

1985) to decadal fluctuations seen in the Greenland ice core records (Taylor et al. 1993).

The THC is associated with deep water formation that occurs in the northern North Atlantic, most importantly in the Greenland–Iceland–Norwegian (GIN) sea region and the Labrador Seas. Substantial interdecadal variability has been observed in the North Atlantic (Levitus 1989; Deser and Blackmon 1993; Kushnir 1994; Hurrell 1995; Dickson et al. 1996). This variability is seen in surface and internal ocean properties, sea ice extent, and atmospheric fields. The long timescale associated with this variability suggests that the ocean and possibly the sea ice systems play an important role.

A hierarchy of modeling studies, from box models (e.g., Stommel 1961) to coupled ocean–atmosphere general circulation models (e.g., Delworth et al. 1993, 1997; Timmermann et al. 1998) have been used to examine the stability and variability of the thermohaline circulation. Many of these studies have found modes of variability on interdecadal timescales that appear to be driven by advective/convective mechanisms (e.g., Mikolajewicz and Maier-Raimer 1990; Weaver et al. 1991; Winton and Sarachik 1993; Delworth et al. 1993; Griffies and Tziperman 1995). The level of ocean–atmo-

* Current affiliation: National Center for Atmospheric Research, Boulder, Colorado.

Corresponding author address: Dr. Marika M. Holland, National Center for Atmospheric Research, P.O. Box 3000, Boulder, CO 80307.
E-mail: mholland@ucar.edu

sphere–ice coupling in these studies appears to have important consequences for the variability. The behavior is complex and it is possible that different mechanisms (including ocean-only and ocean–ice–atmosphere coupled modes) are responsible for the variability obtained in different studies.

This study focuses on the role of sea ice for determining low-frequency variability in the THC. Sea ice processes and Arctic–North Atlantic interactions influence the stability and variability of the thermohaline circulation. Sea ice affects the ocean buoyancy through both thermal and freshwater impacts. It insulates the ocean from the relatively cold atmosphere, causing a reduction in oceanic heat loss. Additionally, the growth (melt) of sea ice results in a net salinity (freshwater) flux.

Perhaps the most important recent example of the effect of sea ice on the variability of the North Atlantic Ocean was the Great Salinity Anomaly (GSA) event. This widespread freshening of the upper 500–800 m of the northern North Atlantic advected around the sub-polar gyre over a 14-yr period starting in the late 1960s (Dickson et al. 1988). Both modeling (Häkkinen 1993) and observational (Walsh and Chapman 1990) studies have concluded that the GSA was largely caused by an increased sea ice export out of the Arctic due to enhanced northerly winds. The thickness of the ice and an increased oceanic transport of freshwater also appear to have played an important role (Häkkinen 1993; Serreze et al. 1992). The GSA resulted in a reduction of deep water formation in the Labrador Sea (Lazier 1980).

Arctic–North Atlantic interactions also appear to play a role in simulated multidecadal THC variability. Using a coupled climate model, Delworth et al. (1997) found that near-surface salinity anomalies in the Arctic and an anomalously strong East Greenland Current preceded temperature and salinity variations in the Greenland sea region. They speculated that the enhanced transport of relatively fresh water and sea ice from the Arctic led to a weakened THC in the North Atlantic. However, they also point out that changes in the THC may have a role in generating the anomalous conditions in the Arctic–Greenland Sea regions.

Several studies have examined the interaction between sea ice and the thermohaline circulation using ocean or ocean–atmosphere models coupled to thermodynamic sea ice models. Using a series of idealized models, Yang and Neelin (1993, 1997) found an interdecadal-timescale, self-sustained ice–ocean coupled mode of variability that is driven by the influence of oceanic heat transport fluctuations on sea ice melt rates and ocean stability. They found that ice–ocean freshwater exchange acts as a negative feedback, causing an oscillatory solution.

Other studies (e.g., Zhang et al. 1995; Lohmann and Gerdes 1998) have found that the insulating capacity of sea ice played the dominant role for determining THC stability. Zhang et al. (1995) obtained a coupled ice–

ocean oscillation with a period of 17 yr. This oscillation was driven by the insulating effects of the sea ice cover and ice–ocean freshwater exchange was shown to be of secondary importance. Lohmann and Gerdes (1998) reached a similar conclusion as to the importance of sea ice for THC stability using an atmosphere–ocean–ice coupled model. All of these studies neglected the seasonal cycle and sea ice dynamics that are both important for determining ice–ocean interactions.

Transport of sea ice from the Arctic to the North Atlantic modifies the ice cover mass balance and, as a consequence, the heat and salinity budgets of the deep water formation regions. The importance of ice dynamics for modifying the THC was discussed by Hasumi and Sugimoto (1995). They used a sector-geometry ocean model coupled to a sea ice model and found that the characteristics of the steady-state THC were substantially different depending on the inclusion of ice dynamics. The influence of variable ice export on the simulated THC was recently addressed by Mauritzen and Häkkinen (1997). They found that the simulated THC depends on the export of sea ice from the Arctic through Fram Strait, with a 2–3 Sv ($1 \text{ Sv} = 10^6 \text{ m}^3 \text{ s}^{-1}$) THC increase corresponding to a decreased ice export of $800 \text{ km}^3 \text{ yr}^{-1}$. Observations show the ice export through Fram Strait to be highly variable (Kwok and Rothrock 1999).

In this study we examine how variability in the Arctic ice pack affects the thermohaline circulation and the general variability of the North Atlantic climate. A global coupled ice–ocean–atmosphere model, described in section 2, is used. This coupled system incorporates an ocean general circulation model, an atmospheric energy–moisture balance model, and a dynamic–thermodynamic sea ice model. Under steady seasonal forcing, an equilibrium solution is obtained that has very little variability. To induce variability within the model system, daily varying wind forcing anomalies are applied to the motion of the Arctic ice pack. This wind forcing is described in section 3. It is obtained from an empirical orthogonal function (EOF) analysis of 40 yr of daily National Centers for Environmental Prediction (NCEP) observations and has the same spatial patterns that are seen in these observations, but with a stochastic time-series. The variability that occurs in the coupled model system is described in section 4.

Several sensitivity runs are examined to determine the effects of sea ice on the coupled system. We examine the effects of the stochastic forcing method by applying stochastic forcing to the ocean freshwater flux instead of the wind stress (section 5). Studies that examine the model sensitivity to the ice–ocean freshwater flux and the ice–ocean heat flux are discussed in section 6. A discussion and conclusions follow in section 7.

2. Model description

The model that is used in this study is a global, coupled climate model based on Fanning and Weaver

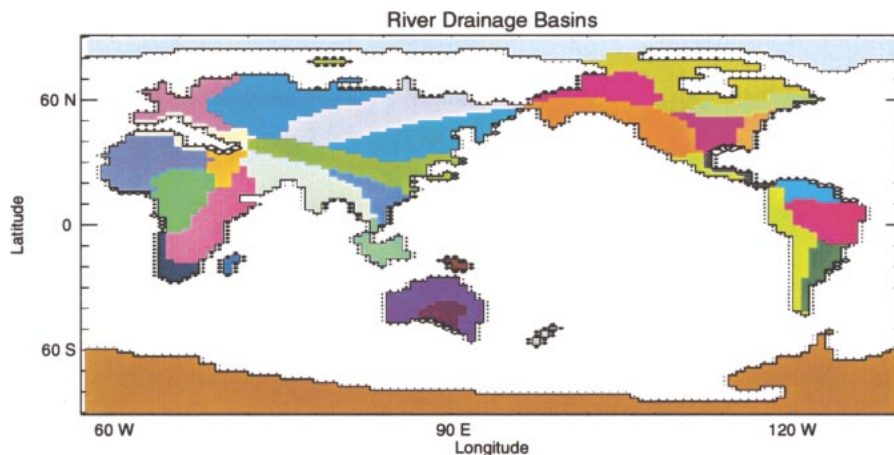


FIG. 1. The model domain and river mask. The model grid has been rotated so that the North Pole lies within Greenland. Thirty-three different river drainage basins are included. The diamonds represent discharge points for the various basins. The discharge points are weighted such that each point drains a fraction of the total corresponding basin discharge. The diamond size represents the discharge weight.

(1996). Several modifications have been made in order to improve the simulated climate with particular attention to the high latitudes. A brief description of the model and modifications is given here.

The ocean model component uses the Geophysical Fluid Dynamic Laboratory's (GFDL) Modular Ocean model, version 2 (Pacanowski 1995). The horizontal resolution is 3.6° longitude by 1.8° latitude. There are 19 vertical levels, varying in depth from 50 m near the surface to approximately 500 m at depth. Realistic geography and bathymetry (within the limitations of the model resolution) are used. The Bering Strait and Canadian Arctic Archipelago are closed due to the coarseness of the resolution. A 12-h time step is used to solve the tracer equations while an 18-min time step is used to solve the momentum equation. The level of time splitting used here has been tested and shown to not affect the simulated variability. A depth-dependent vertical diffusivity is used in the model. It has been slightly modified from Bryan and Lewis (1979) so that a higher diffusion is used. It ranges from $k_v = 0.6 \times 10^{-4} \text{ m}^2 \text{ s}^{-1}$ at the surface to $k_v = 1.6 \times 10^{-4} \text{ m}^2 \text{ s}^{-1}$ at depth. A constant horizontal viscosity and diffusivity of $A_h = 2.0 \times 10^5 \text{ m}^2 \text{ s}^{-1}$ and $k_h = 2.0 \times 10^3 \text{ m}^2 \text{ s}^{-1}$, respectively are used. The vertical viscosity is held fixed at $A_v = 1.0 \times 10^{-3} \text{ m}^2 \text{ s}^{-1}$.

The atmospheric component of the coupled model is an energy–moisture balance model (EMBM) with no explicit atmospheric dynamics. It is run on the same horizontal grid as that used in the ocean model. Heat and water vapor transports are parameterized as diffusive processes. The atmosphere and ocean are coupled through the exchange of heat and freshwater. Precipitation occurs when the relative humidity in the atmosphere reaches a threshold value of 0.85. Rainfall over land instantaneously runs back into the oceans based on

a specified river basin mask that incorporates 33 different drainage basins. (Fig. 1). Snowfall is allowed to accumulate on the land unless the air temperature is above -5°C . At this temperature snow melts at a specified melt rate of $0.5 \text{ cm day}^{-1} \text{ }^\circ\text{C}^{-1}$. The planetary albedo is parameterized as a function of latitude and time of year (Graves et al. 1993). The presence of snow cover or sea ice locally increases the planetary albedo by 0.18.

Because the EMBM contains no explicit atmospheric dynamics, the surface momentum forcing of the ice and ocean is applied through a specified wind stress. In general, a monthly climatology based on NCEP reanalysis data is used for this forcing. However, as described below, daily wind stress anomalies are added to the climatological momentum forcing of the ice cover in order to induce variability within the model. In addition to surface wind stress, the model is forced with seasonally varying incoming solar radiation. No flux adjustments are used in the simulations.

A dynamic sea ice formulation that uses an elastic–viscous–plastic rheology (Hunke and Dukowicz 1997) is included in the current model. This model has a sub-grid-scale ice thickness distribution that resolves 10 ice categories within each model grid cell (Hibler 1980; Flato and Hibler 1995). The presence of an ice thickness distribution affects the ice–ocean–atmosphere fluxes and the net ice growth rates (e.g., Maykut 1982; Holland et al. 1997). The relatively simple Semtner (1976) zero-layer thermodynamics is used to solve for the ice surface temperature and ice growth rates.

A rotation of the model grid (Fig. 1) is employed in order to avoid the problem of converging meridians over the Arctic Ocean. A simple Euler angle rotation is used to displace the North Pole 13° south into Greenland while the South Pole remains within the Antarctic con-

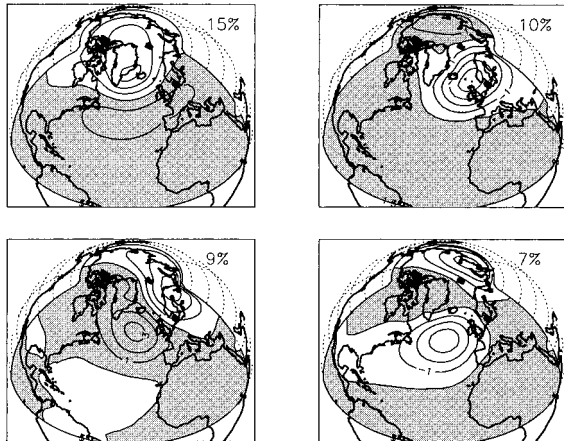


FIG. 2. The first four EOFs of NCEP daily surface pressure data. The percent of the variance represented by each EOF is shown in the upper-right corner.

continent (Eby and Holloway 1994). As a consequence, the zonal grid lines no longer lie along lines of latitude but are instead shifted. The grid rotation better resolves processes operating within the Arctic with minimal impact on the rest of the globe.

3. Experimental design

In order to force variability within the model, daily stochastic forcing is applied to the wind stress over the sea ice cover. The ocean surface is not affected directly in this process, because a climatological wind stress is applied over the ocean (and to the ocean underneath the ice pack). This means that momentum is not conserved in the ice–ocean coupling. However, it simplifies the interpretation of the results and allows for relatively long time steps in the ocean model. Any simulated ocean variability is a result of buoyancy forcing from sea ice, because the momentum exchange is constant from one year to the next.

We construct stochastic forcing by summing a set of observed spatial sea level pressure (SLP) anomaly patterns multiplied by stochastic time series. The resulting stochastic SLP anomaly fields are subsequently converted into surface geostrophic winds. The spatial patterns are derived from an EOF analysis of daily 1958–97 NCEP reanalysis over a region consisting of the Arctic and North Atlantic (see Fig. 2). We use the leading 20 EOFs that explain 83% of the variance of the observed SLP. The stochastic expansion coefficients for the spatial patterns are modeled using a discrete first-order Markov process with parameters designed to reproduce statistically the variance of the observed principal components. The resulting forcing field is random in time, but has a spatial pattern that is similar to observations. The absence of any preferred timescales in the forcing means that the preferred timescales that oc-

cur in the model simulations are due to internal model physics and not to external forcing.

A standard simulation is run in which all ice–ocean–atmosphere feedback mechanisms are active. Sensitivity tests are then used to examine the impact of the ice–ocean forcing on the simulated variability. We also test the model sensitivity to the method of stochastic forcing by applying stochastic forcing to the freshwater flux over the primary ice melt region in the GIN Seas instead of to the ice motion. The standard simulation is run for 1000 yr from initial conditions that are obtained from a 2500-yr spinup run in which no stochastic forcing is applied. Once stochastic forcing is applied in the model, few trends arise and the mean climate changes little.

4. The standard simulation

Here we discuss the standard simulation of the coupled model. As mentioned above, the variability in this simulation is forced by applying daily wind stress anomalies in addition to the climatological fields that are used to force the motion of the Arctic ice pack. Results from a 1000-yr-long integration of the coupled model are discussed.

a. Climatology

Here we discuss the climatology of the Arctic and North Atlantic that are directly relevant to the variability produced in the model. All of the mean fields have been averaged over 100 yr of integration and are shown for the standard simulation.

The climatological mean ocean temperature (SST), salinity (SSS), and currents at 25-m depth over the North Atlantic are shown in Fig. 3. The SST and SSS are reasonable compared to observations. However, there are several problems that are likely due to the relatively coarse resolution of the ocean model. For example, the North Atlantic Drift that brings warm water into the Norwegian Sea is somewhat weak. This weak flow results in too little heat transport into this region and affects the wintertime sea ice edge. The latitude of the Gulf Stream separation varies with the fluctuations in the THC. During years of strong circulation, the latitude shifts southward due to a strengthening of the subpolar gyre. In the climatological mean, the separation from the North American coast occurs south of Newfoundland, which is north of the observed separation near Cape Hatteras. This average separation location is similar to that in the 2500-yr spinup run.

The average ice thickness and ice drift for the Northern Hemisphere are shown in Fig. 4. In general agreement with observations (Bourke and Garret 1987), the ice cover reaches a maximum thickness in excess of 6 m along the north Greenland coast and the Canadian Arctic Archipelago. The simulated ice cover is more extensive than observed during winter with seasonal ice cover seen in the Norwegian and Barents Sea regions.

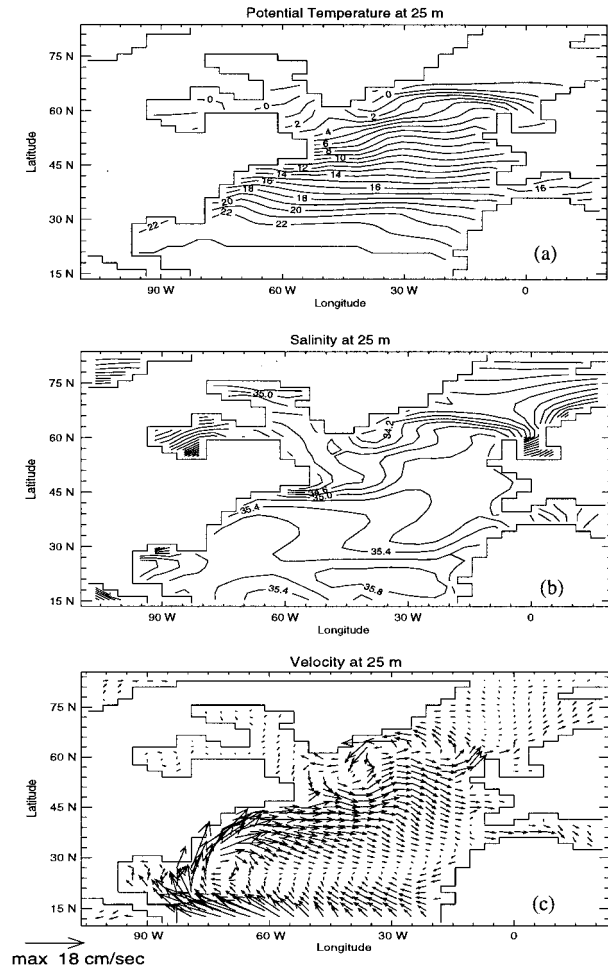


FIG. 3. The average (a) SST in $^{\circ}\text{C}$, (b) SSS in ppt, and (c) ocean currents in the North Atlantic. The SST and SSS contour intervals are 1°C and 0.2 ppt, respectively.

This is a common problem in many coarse-resolution coupled models and is almost certainly due to the relatively low oceanic heat transport into the GIN sea region as mentioned above. The transport of the ice pack is reasonable and has a well-developed Beaufort gyre and transpolar drift stream. The freezing rates (Fig. 5) also appear reasonable with net freezing occurring over the central Arctic and net melting occurring in the Greenland and Labrador Sea regions.

The ice cover affects the global thermohaline circulation through ocean buoyancy forcing. Relatively fresh sea ice is advected into and melts in the deep water formation region, causing a freshening of the water column. Sea ice also insulates the ocean from the overlying cold atmosphere, reducing the oceanic turbulent heat loss. These different mechanisms and the role that they play in the variability of the thermohaline circulation are discussed further in section 6.

The average meridional overturning streamfunction for the North Atlantic is shown in Fig. 7, revealing a maximum value of approximately 24 Sv. The dominant

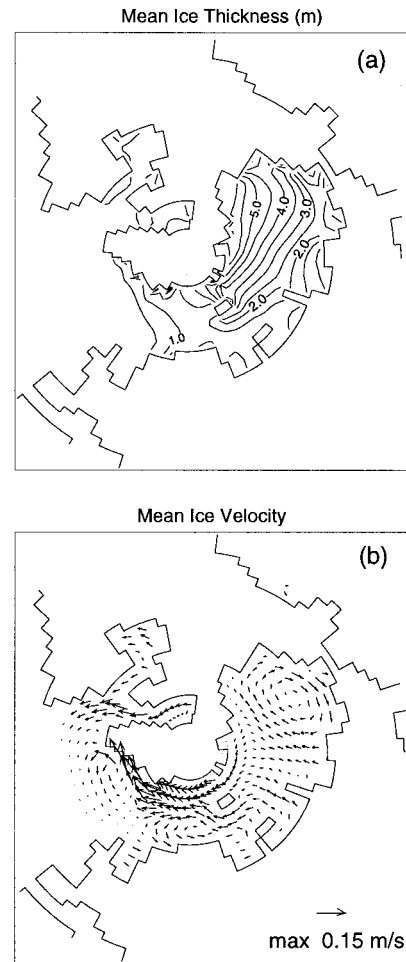


FIG. 4. The average (a) ice thickness in m and (b) ice velocity for the Northern Hemisphere.

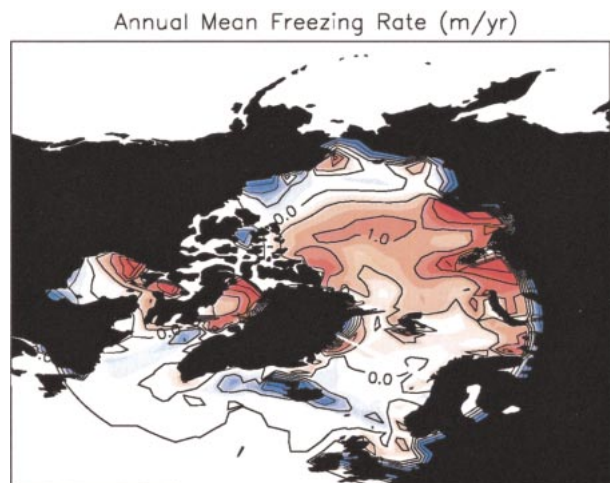


FIG. 5. The average freezing rate in m yr^{-1} for the Northern Hemisphere. The contour interval is 0.5 m yr^{-1} .

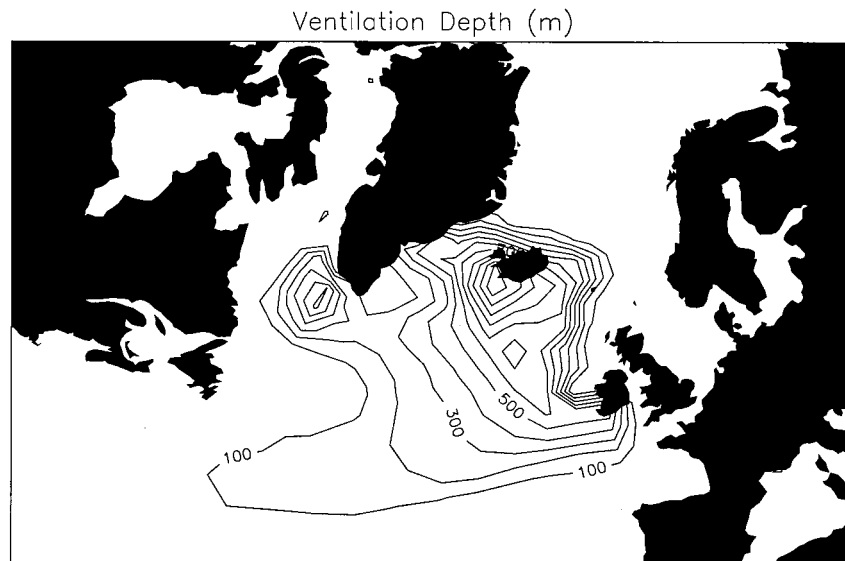


FIG. 6. The average ventilation depth in m in the North Atlantic. The contour interval is 100 m. The ventilation depth is computed as the depth to which convective adjustment occurs.

convective site occurs to the south of Denmark Strait (Fig. 6) and has a maximum average ventilation depth of approximately 1200 m. Other deep water formation sites occur in the Labrador Sea and the central Arctic. Very little deep water forms in the GIN sea region. This is linked to the presence of seasonal ice cover in the region and likely results from the inadequate resolution of the North Atlantic drift and the poor parameterization of, for example, subgrid-scale mixing (Gent and McWilliams 1990), small-scale brine rejection (Duffy et al. 1999), and the bottom boundary layer (Beckmann and Doeschner 1997).

We are interested in the variability that occurs in the overturning circulation and its link to the ice cover. In order to examine the overturning variability, an overturning index is defined as the annual average maximum value of the North Atlantic meridional streamfunction.

The time series and spatial patterns of the variability are discussed below.

b. North Atlantic variability

1) OCEANIC VARIABILITY

The time series and spectrum of the overturning index is shown in Fig. 8. The overturning index has a standard deviation of approximately 1.9 Sv and throughout the time series several “extreme” events occur with anomalies greater than 5 Sv (approximately 20% of the mean). The overturning index spectrum has higher power at lower frequencies that is characteristic of a red spectrum. However, in comparison to a theoretical red spectrum with the same variance, there are some considerable differences. In particular, the overturning index has enhanced power at interdecadal timescales, with a spectral peak at approximately 20 yr.

The North Atlantic overturning cell exhibits both a strengthening/weakening over time and a north/south shift. This can be seen in the first two EOFs of the North Atlantic meridional streamfunction (Fig. 9). The leading EOF, which accounts for 82% of the variance, has a monopole structure that represents the strengthening/weakening of the overturning cell. It is essentially the spatial representation of the overturning index and is highly correlated to this index. The second EOF, which accounts for 12% of the variance, has a dipole structure that represents a latitudinal shift in the overturning cell. It is correlated to the overturning index, with a northward shift in the overturning cell leading a high overturning index by 2 yr and a southward shift lagging a high overturning index by 6 yr. The northward shift in the overturning cell is coincident with a northward shift

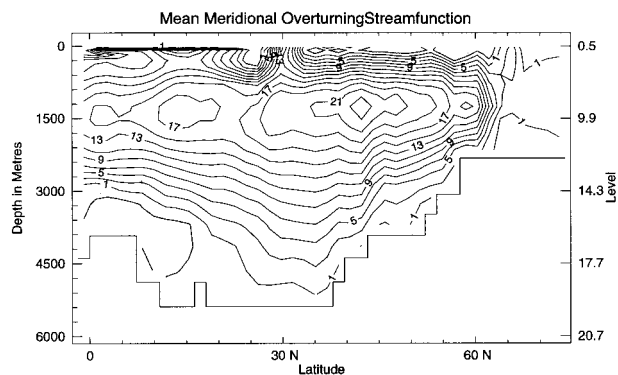


FIG. 7. The average meridional overturning streamfunction for the North Atlantic in Sv. The contour interval is 2 Sv and negative values are shaded.

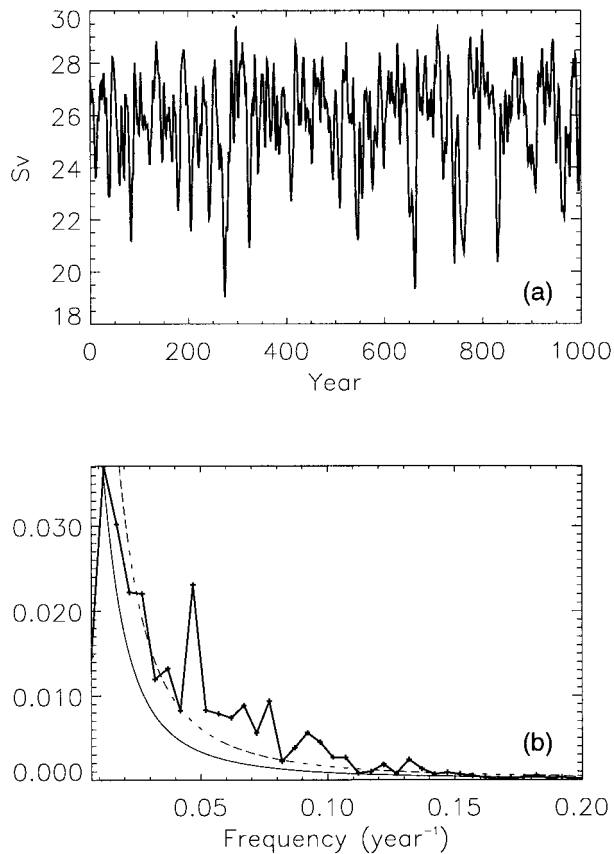


FIG. 8. The (a) time series in Sv and (b) spectrum of the annual-averaged overturning index. In (b), the thin solid line denotes the theoretical red spectrum and the dashed line is the 95% significance level. The spectrum for this and all following figures is computed using a hamming window.

in the ice edge. Both overturning EOFs have enhanced power at interdecadal timescales. Similar patterns of the meridional streamfunction are seen in the variability present in the GFDL coupled model (Griffies and Bryan 1997) and in the National Center for Atmospheric Research (NCAR) Climate System Model (Capotondi and Holland 1998).

The variability seen in the overturning circulation is related to changes in the sea surface temperature and salinity. The leading EOF of SST and SSS represent 46% and 50% of the variance, respectively, and are correlated to each other at 0.96. They have a largely monopolar structure centered south of Greenland (Fig. 10) with small anomalies of opposite sign occurring off Newfoundland. The pattern of these EOFs is similar to that seen in other modeling studies (Griffies and Bryan 1997; Capotondi and Holland 1998). These surface ocean conditions are highly correlated to the overturning index (at greater than 0.8) with warm and saline conditions preceding a high overturning state by approximately 2 yr. This suggests that these ocean conditions force the overturning variability.

Figure 11 shows the coefficients of the density lin-

early regressed on the overturning index for the total density and the density components due to variable salinity and temperature. These regression coefficients were obtained from 100 yr of model output and were averaged vertically and horizontally over the primary convective region (defined as a region across the northern North Atlantic from approximately 50° to 70°N). As expected from the EOF analysis, the salinity-forced density changes are largely responsible for changes in the stability of the water column. Temperature effects act as a damping to the initial density perturbation, causing the total column density anomaly to decrease more rapidly following a high overturning state. This negative feedback from temperature anomalies is similar to what has been seen in the ocean box model experiments of Griffies and Tziperman (1995).

A regression of the ocean surface heat and salinity budgets on the overturning index is shown in Fig. 12. The changes in SSS that drive the overturning variability are induced by variations in the surface freshwater flux. Four years prior to a high overturning event, the surface salinity flux is large (Fig. 12b). The resulting high SSS destabilizes the water column and enhances convection. Vertical mixing warms the surface ocean (Fig. 12a). As the overturning strength increases, the northward advection of heat also increases, enhancing the initial SST changes. Due to the warm ocean temperatures, there is above-normal heat loss to the atmosphere that results in relatively warm air temperatures over the convective regions. As shown in Fig. 11, the changes in ocean temperature act as a negative feedback on the overturning variability.

2) INFLUENCE OF THE ICE COVER

As we are stochastically forcing the ice motion, it is reasonable to expect that the variable surface fluxes that instigate the overturning changes are a result of changes in ice export and consequent melting in the northern North Atlantic. Figure 13 shows the time series, spectrum, and correlation to the overturning of the anomalous ice export through the Fram Strait–Barents Sea region. The mean Arctic ice export throughout the integration is approximately 3100 km³ yr⁻¹ with a standard deviation of 1200 km³ yr⁻¹. This compares well to the mean export of 2800 km³ yr⁻¹ that is seen in the observational record (e.g., Aagaard and Carmack 1989; Vinje et al. 1998). The variability in the simulated ice export also appears reasonable compared to the limited observations.

The smoothed Arctic ice export is anticorrelated to changes in the overturning at 0.75 when it leads the overturning time series by 4–5 yr consistent with the salt flux lead times of Fig. 12. The spectrum of the export time series is relatively white, although significant variability (at greater than 95% significance level compared to the theoretical spectrum) occurs at several frequencies, including $f \approx (23 \text{ yr})^{-1}$, which is similar

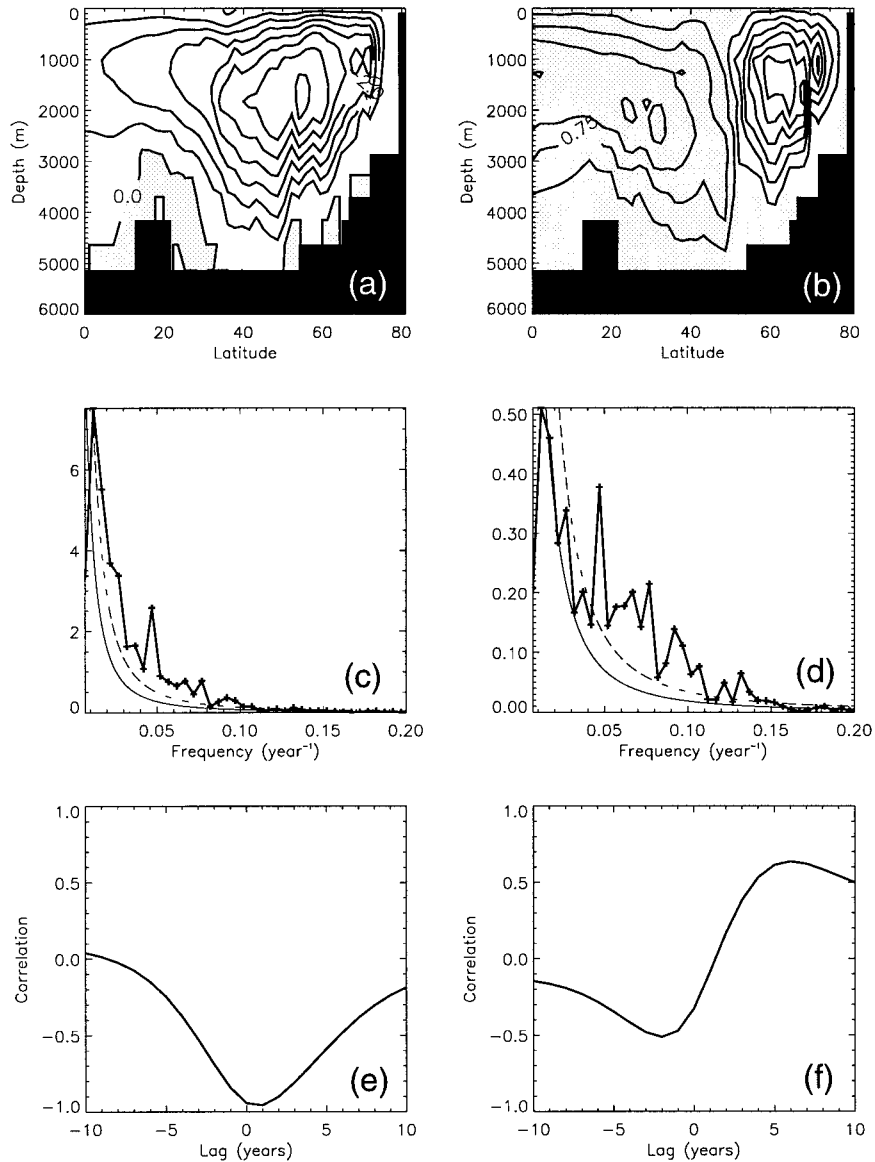


FIG. 9. The (a) first and (b) second EOF of the annual-averaged meridional overturning streamfunction. The EOFs have been normalized by their standard deviation. Positive contours are shaded. Also shown in (c) and (d) are the spectra of the principal components of the first and second EOFs, respectively, and in (e) and (f) their correlation to the meridional overturning index. A negative (positive) lag implies that the principal component time series leads (lags) the overturning index.

to the timescale of the variability seen in the overturning index. Ice is also exported from Baffin Bay into the northern North Atlantic. This appears to play a role in the variability of the Labrador Sea ice cover. However, it has a negligible effect on the overturning circulation variability.

The ice export from the Arctic is a function of both the velocity and the thickness of ice leaving the Arctic Basin:

$$\text{export} = \int (\bar{u}\bar{h} + \bar{u}h' + u'\bar{h} + u'h') ds, \quad (1)$$

where u represents the ice velocity and h represents ice thickness. The integral in Eq. (1) spans the distance between Greenland and Norway. An overbar indicates the mean value and a prime indicates the deviation from this mean. The importance of ice velocity versus ice thickness perturbations for determining the timescale of the variability is shown in Fig. 14. The high-frequency changes in ice export are largely driven by ice velocity anomalies. Variations in ice thickness become important for low-frequency variability in the ice export. Export variability at periods longer than approximately 15 yr

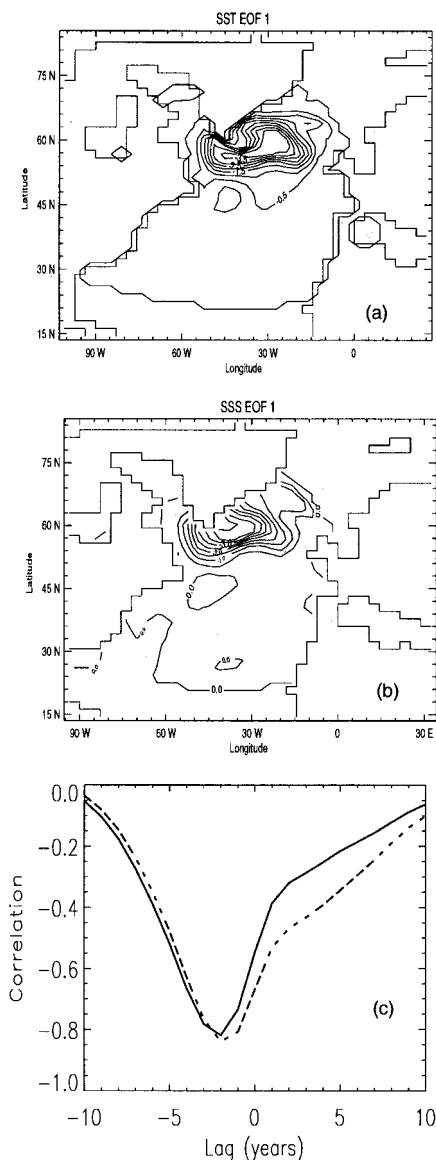


FIG. 10. The leading EOF of annual-averaged (a) SST and (b) SSS. (c) The correlation between the overturning index and the principal components of the first EOF of SST (dashed line) and SSS (solid line). A negative lag implies that the principal components lead the overturning index.

is equally forced by anomalies in the ice thickness and ice velocity.

Ice export influences the GIN Seas freshwater flux, by providing variations in the ice volume that is available for melting in this region. Figure 15 shows the regression between the overturning and the northern North Atlantic ice growth rates for the annual average and different seasons. Anomalous summer ice melt primarily affects the upper layers of the water column due to the lack of deep convection during this time. The resulting surface salinity anomalies then influence convection the following winter. In contrast, variations in

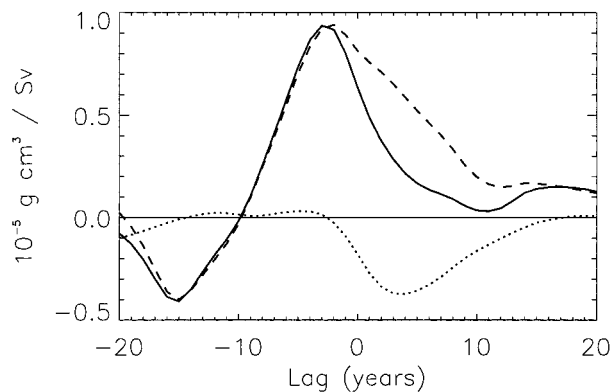


FIG. 11. The coefficients of density linearly regressed on the overturning index as a function of lag. The regression coefficients are vertically and horizontally averaged over the primary convective region. Shown are the regressions of the total density (solid line), the component due to variable temperature (dotted line), and the component due to variable salinity (dashed line). A negative lag implies that density perturbations lead changes in the overturning index.

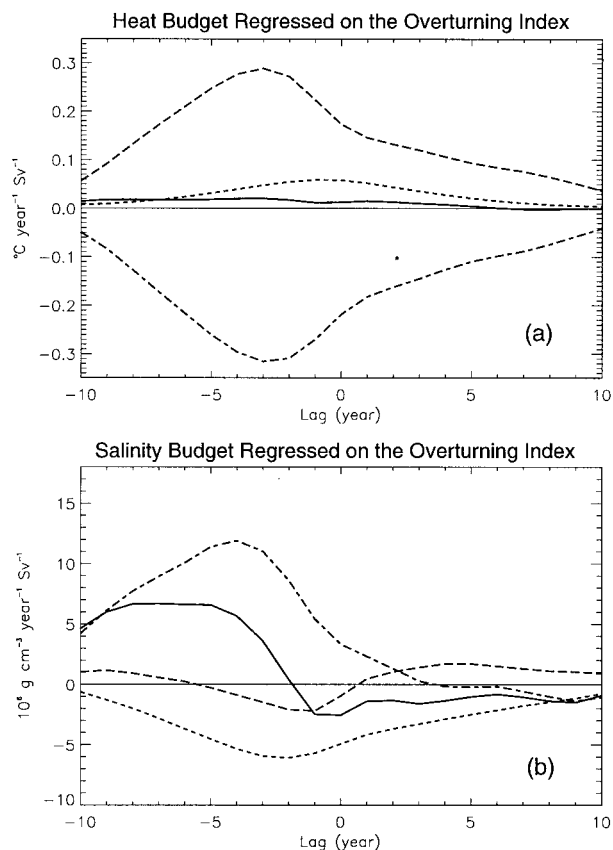


FIG. 12. Linear regression coefficients of (a) heat and (b) salinity budgets regressed on the overturning index as a function of lag. The heat and salinity budgets are for the surface of the northern North Atlantic from approximately 57° to 75°N . The terms shown are the total (solid line), horizontal processes (dotted line), vertical processes (dashed line), and surface fluxes (dot-dashed line). The horizontal processes include advection and diffusion. The vertical processes include advection, diffusion, and convection (of which convection is the dominant term).

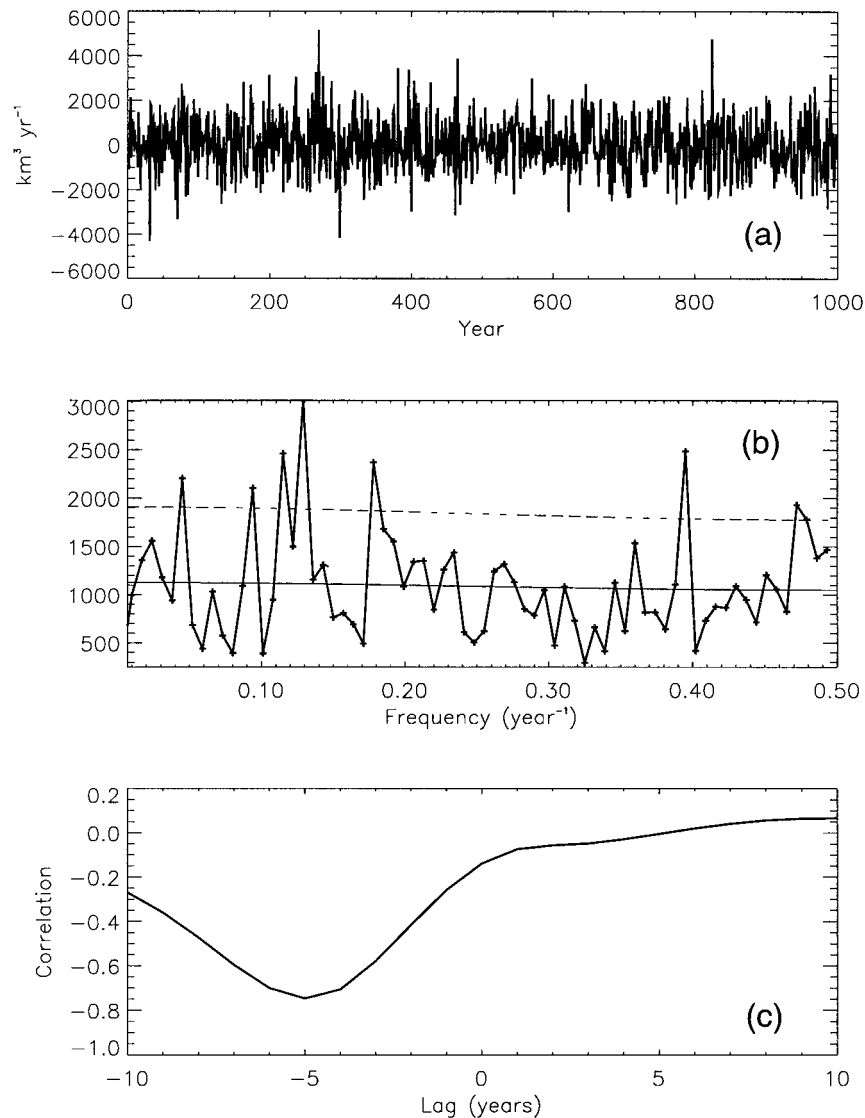


FIG. 13. The (a) time series, (b) spectrum, and (c) correlation to the overturning index of anomalous annual-averaged ice export from the Arctic. (b) The thin solid line denotes the theoretical spectrum and the dashed line denotes the 95% significance level. (c) A negative lag implies that the export leads changes in the overturning. The ice export time series was smoothed with a 5-yr running mean to obtain the correlation coefficients.

the brine rejection during winter ice growth are mixed down in the water column. The annual average ice growth is anomalously high approximately 4–10 yr preceding a high overturning anomaly. From Fig. 15, we see that this is largely driven by below-average summer melt rates that are linked to low ice export. The reduced freshwater flux caused by the negative melt anomalies enhances convection the following winter that, as discussed above, warms the surface ocean. This additional heat that is available to the ice cover results in anomalously low wintertime ice growth rates. Coincident with and for several years after the positive overturning anomaly, the anomalously low wintertime ice growth rates dominate, causing below-average annual ice

growth to occur. Ultimately, these below-average growth rates act to freshen the water column, stabilizing the surface ocean and decreasing the overturning. This acts to damp the initial change in the THC. The strength of this damping mechanism is analyzed in the sensitivity tests discussed in section 6.

In our simulations, the ice export is important for providing the initial impulse to the system, causing a change in the freshwater flux in the northern North Atlantic and subsequently in the overturning strength. Because of damping in the system, variable forcing must be supplied continuously to sustain the THC variability. After the initial impulse, the ice–ocean coupling becomes important for determining and damping the var-

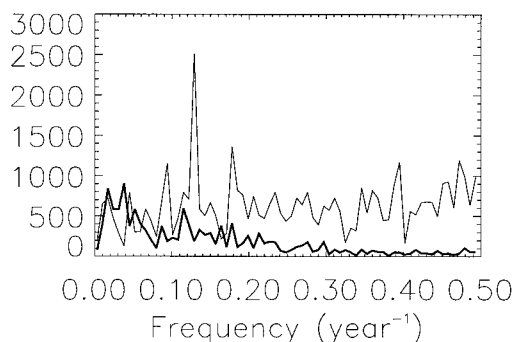


FIG. 14. The spectrum of the components of ice export due to velocity changes, $\int (u'h) ds$ (thin line) and due to ice thickness changes, $\int (\bar{u}h') ds$ (bold line).

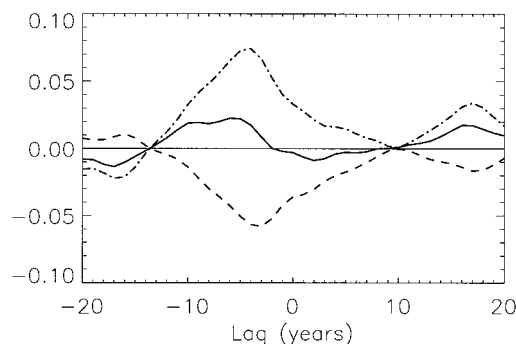


FIG. 15. Coefficients of the GIN Sea ice growth rate anomalies linearly regressed on the overturning index as a function of lag. Shown are values for the total annual growth rate (solid line), the growth rate during the melt season (May–Aug; dot–dash line), and the growth rate during the growth season (Sep–Apr; dashed line). A negative lag implies that the ice growth rates lead changes in the overturning. Note that “positive growth rate anomalies” are equivalent to negative melt rate anomalies.

iability. As shown in previous studies (Griffies and Tziperman 1995; Delworth et al. 1993), changes in the ocean heat transport also appear to damp the overturning variability. The importance of the ice–ocean coupling for determining the variability will be addressed further in the sensitivity studies described in section 6. All of the model experiments are described in Table 1.

5. Sensitivity to stochastic freshwater forcing

It is possible that the preferred timescales of the THC variability are forced by anomalies that originate within the Arctic Basin and are exported into the North Atlantic with the ice drift. Alternatively, the preferred low-frequency timescales in the ice export may be driven by THC variability that is dependent on stochastic forcing (in the form of ice export) to be sustained. THC variability does appear to impact the Arctic Basin. For example, changes in heat transport into the Arctic Basin associated with THC variability are clearly seen in the regression of Arctic Ocean temperature on the overturning time series (Fig. 16). High Arctic temperatures lead and are coincident with an increase in the overturning index. This impacts the ice growth rates in the Arctic Basin and leads to preferred timescales in the ice thickness and consequently, the ice export, which are similar to the THC variability.

In experiment STOCH_FW, the model sensitivity to

the source of the stochastic forcing is examined by applying a constant annual cycle of wind forcing to the ice momentum budget and stochastic perturbations to the oceanic freshwater flux over the ice melt regions (Fig. 17). Previous studies (e.g., Weisse et al. 1994; Capotondi and Holland 1997) have shown that stochastic freshwater forcing excites THC variability. In this sensitivity test we wish to examine if the sea ice forced variability of the control run is consistent with a purely random freshwater forcing mechanism. The stochastic forcing that is applied in this sensitivity test is modeled using a first-order autoregressive process and has a similar standard deviation and seasonal cycle to the ice export variability obtained in the standard simulation. Thus, the stochastic forcing applied in this case is meant to be representative of the random forcing element of the freshwater impact of the ice export anomalies seen in the standard simulation (assuming that the ice export anomalies are immediately converted into freshwater flux anomalies). The simulation is run for 1000 yr from initial conditions obtained from the standard simulation. The results from this sensitivity test will help to determine if the preferred timescales of the

TABLE 1. The different model experiments discussed in the text.

Experiment name	Stochastic forcing	Description	Run length (yr)
Standard	Wind stress	All feedbacks are active	1000
STOCH_FW	Freshwater flux	All feedbacks are active	1000
NO_FWFLX1	Wind stress	No ice–ocean freshwater flux feedbacks Annually periodic freshwater ice–ocean exchange is used	1000
NO_FWFLX2	Freshwater flux	No ice–ocean freshwater flux feedbacks Annually periodic freshwater ice–ocean exchange is used	500
NO_HFLX	Wind stress	No ice–ocean heat flux feedbacks Annually periodic ice–ocean heat exchange is used	1000

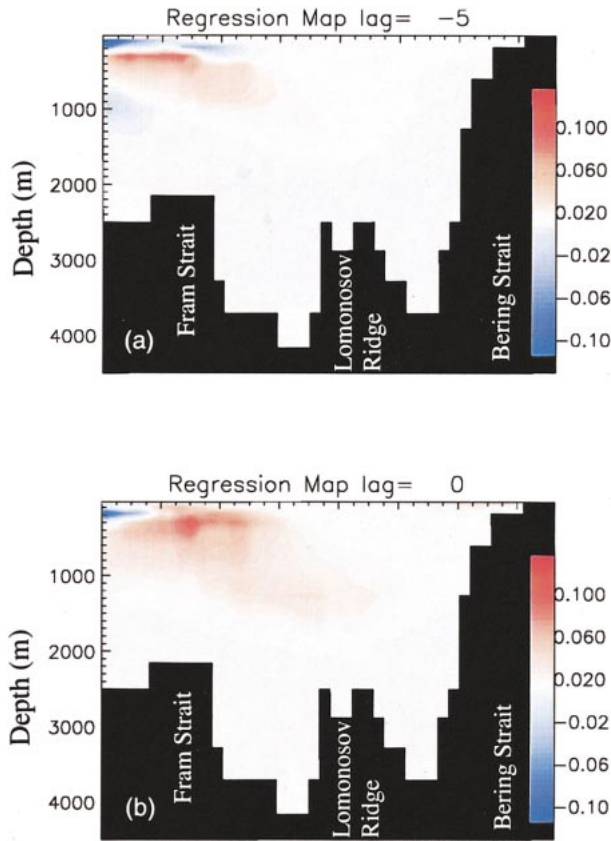


FIG. 16. The linear regression coefficients of a section of potential temperature across the Arctic Basin regressed on the overturning index for (a) 5 yr preceding the overturning and (b) coincident with the overturning. The units are in $^{\circ}\text{C Sv}^{-1}$.

THC variability are dependent on internal Arctic processes.

Figure 18 shows the time series and spectrum of the overturning index in experiment STOCHFW. The standard deviation of the overturning time series is approximately 1.8 Sv, which is similar to the standard deviation of 1.9 Sv from the standard simulation. The timescales of this variability are also similar to the standard simulation. In particular, a well-defined spectral peak, with a similar amount of variance, occurs at a 20–25-yr timescale. Enhanced variability is also present at lower frequencies. In the sensitivity test, this variability is largely concentrated at approximately 35 yr, whereas in the standard simulation it is more broadly distributed. The leading EOF of the meridional overturning streamfunction (not shown) has the same monopolar structure as the leading EOF from the standard case (Fig. 9a). However, in contrast to the standard simulation, over 99% of the variance is represented by this spatial mode (as compared to 85% in the standard case) and the EOF that represents a north–south shift in the overturning circulation (Fig. 9b) is not present.

Variability in the SST and SSS appears to be similar to the standard simulation. For example, the leading

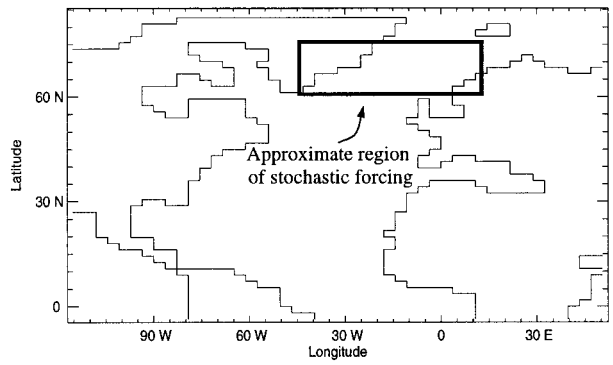


FIG. 17. The approximate region where stochastic forcing is applied in experiment STOCHFW.

EOF of SST and SSS (not shown) resembles Fig. 10. As in the standard simulation, approximately 4 yr prior to a high overturning index, the surface oceanic flux of salinity is anomalously high. This destabilizes the water column, causing enhanced convection and warmer ocean temperatures.

Based on the similarities in the timescales and patterns of the variability and the surface ocean conditions in the North Atlantic, we believe that the 20–25-yr mode of THC variability in STOCHFW arises from similar

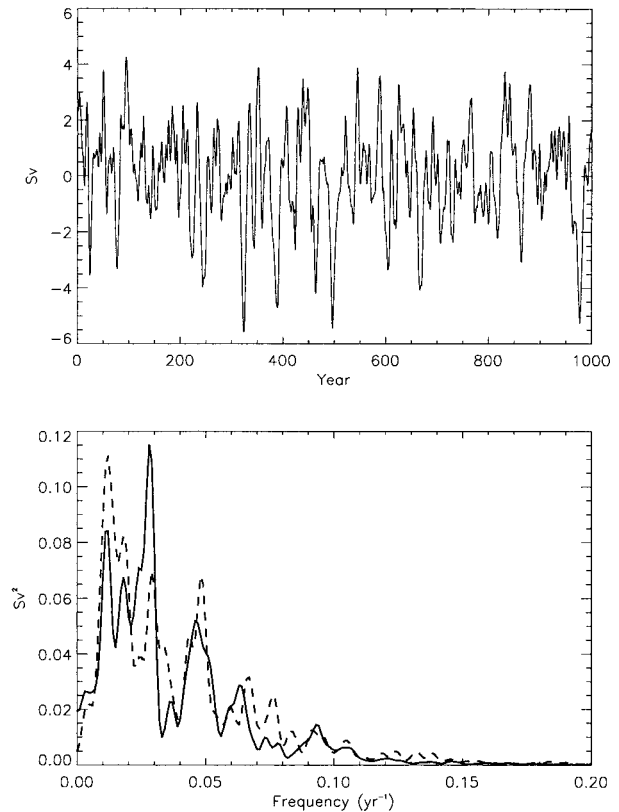


FIG. 18. The (a) time series and (b) spectrum of the overturning index obtained in experiment STOCHFW. Also shown in (b) is the spectrum obtained in the standard simulation (dashed line).

TABLE 2. The standard deviation of the annually averaged ice volume, ice export, and overturning index for the standard case and sensitivity tests. The sensitivity tests are described in Table 1.

Lab ice volume (km ³)	109.9	63.8	22.7	199.3	24.9
GIN ice volume (km ³)	931.9	392.0	509.4	870.9	366.9
Ice export (km ³ yr ⁻¹)	1211	31	1186	47	996
Overturning index (Sv)	1.86	1.76	0.08	2.45	2.43

mechanisms to those in the standard case. In both the standard case and STOCHFW, the surface freshwater flux drives changes in the stability of the water column. These freshwater flux anomalies are caused by different mechanisms in the two simulations. In the standard simulation the anomalies are largely a result of changes in ice growth/melt in the northern North Atlantic that are led by changes in Arctic ice export, whereas in STOCHFW stochastic anomalies are applied to the freshwater flux. In STOCHFW, the ice export variability is almost annually periodic (Table 2).

The coefficients of the different components of the surface freshwater flux regressed on the overturning in-

dex is shown in Fig. 19. High values of the applied stochastic salinity flux lead a high overturning index by approximately 4 yr. The stochastic component has a large impact on the THC variability, compared to the ice melt component. The ice melt counteracts the stochastic flux, acting to damp changes in the overturning. As occurs in the standard simulation, large changes are seen in the relationship between the overturning and the ice growth/melt for different seasons. In particular, low summertime ice melt acts to reinforce the high stochastic salinity flux that leads a high overturning index. The winter ice growth rates counteract the summertime ice melt and stochastic freshwater forcing terms. The impact of the seasonal ice growth rates on the freshwater flux have a maximum regression value approximately a year after the maximum stochastic flux regression. This implies that the stochastic forcing term (much like the ice export in the standard simulation) provides the initial “kick” to the system, modifying the oceanic conditions, which in turn affect the ice growth/melt rates in the northern North Atlantic.

The Arctic Basin is relatively quiescent in experiment STOCHFW. Figure 20 shows the ice thickness standard deviation that results from the 1000-yr-long integration. There is little variability in the ice thickness within the Arctic Basin. However, the ice thickness variability along the ice edge off the southeastern coast of Greenland is nearly identical to that obtained in the standard simulation (Fig. 21). As we will show below (section 6b), the variability in this region is driven by changes in the local ice melt rates due to variable ocean heat flux. Although the THC variability does not appear to be dependent on internal Arctic processes, it is still possible that ice–ocean coupling within the northern North Atlantic is necessary for determining the overturning variability. This will be addressed further in section 6.

Variability in the Arctic ice pack in the standard simulation is largely forced by the presence of variable winds. Consequently, the Arctic ice thickness variability is weak in experiment STOCHFW because the winds are annually periodic (Fig. 20). However, in both the standard simulation and this sensitivity test, changes in the THC force low-frequency variability in the ice thickness in Fram Strait. In the sensitivity test, this causes the ice export time series (which generally has relatively low variability), to have enhanced power at interdecadal timescales (not shown) due to changes in the heat transport into the Arctic. It is likely that a similar mechanism is responsible for the low-frequency variability in the ice export time series for both simulations.

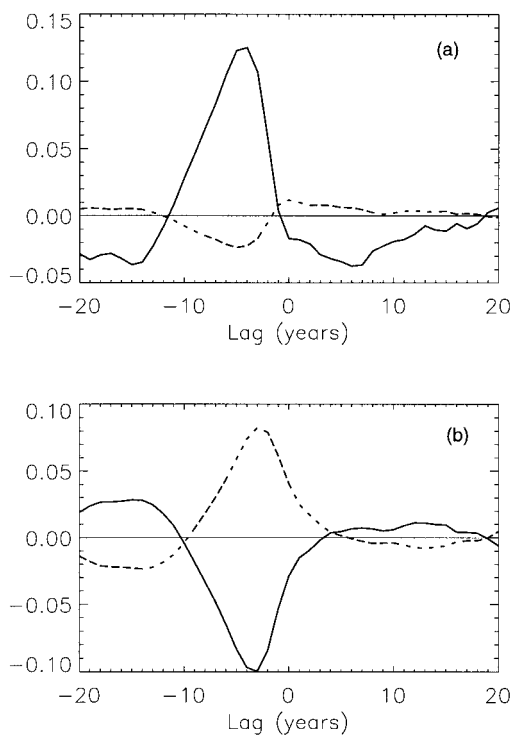


FIG. 19. (a) Coefficients of the components of the GIN Sea negative surface freshwater flux linearly regressed on the overturning index as a function of lag. A negative lag implies that the freshwater flux leads changes in the overturning index. Shown are the stochastic component (solid line) and the ice melt term (dashed line). Precipitation–evaporation is not shown, but it is negligible. (b) The linear regression coefficients of the seasonal components of the negative freshwater flux due to ice melt regressed on the overturning index as a function of lag. The solid line represents the winter (Sep–Mar) ice growth and the dashed line represents the summer (Apr–Aug) ice growth (negative ice melt). A regression of the negative surface freshwater flux is used for comparison with Fig. 15. The units are in Sv/Sv.

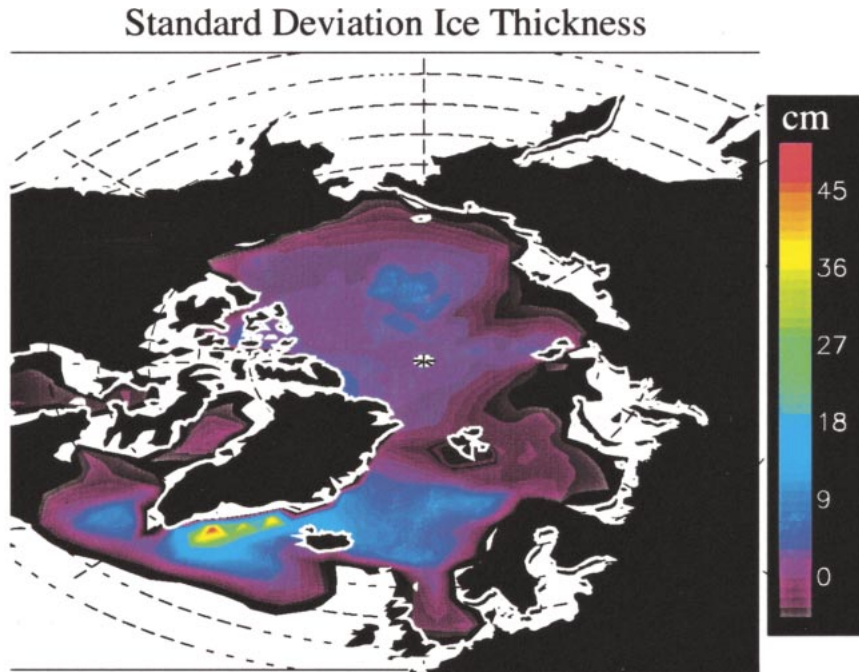


FIG. 20. The standard deviation of annual-averaged ice thickness obtained in experiment STOCHLFW.

Two additional simulations have been run to examine the sensitivity of the THC variability to the timescale of the stochastic forcing. In the first experiment, the stochastic freshwater anomalies are low-pass filtered such that variability with periods shorter than 10 yr is

removed. In the second experiment, the stochastic freshwater anomalies are high-pass filtered, removing variability at periods longer than 10 yr. These simulations, which are run for 500 yr, allow us to determine whether the THC variability is a resonant response to a limited

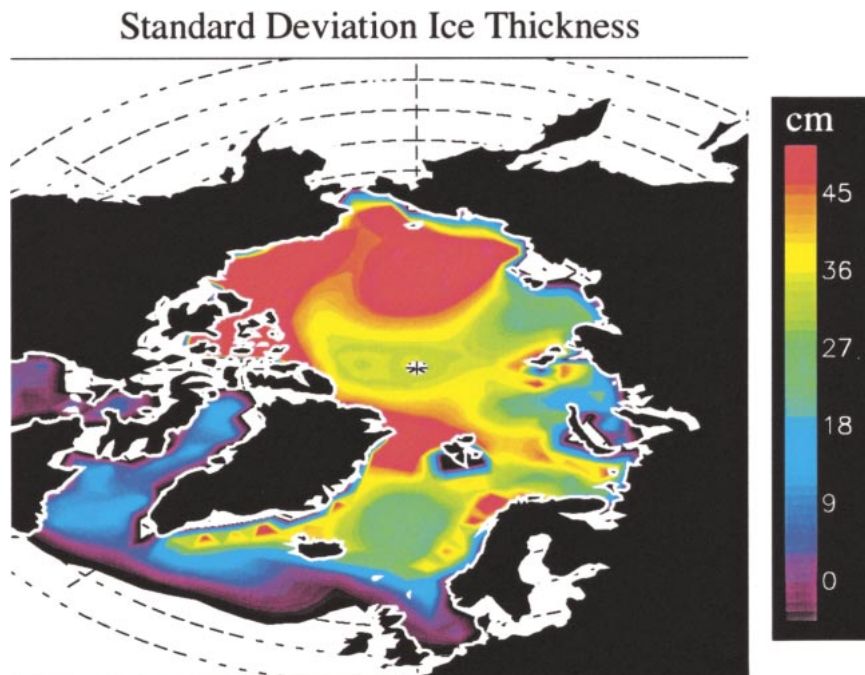


FIG. 21. The standard deviation of annual-averaged ice thickness obtained in the standard case.

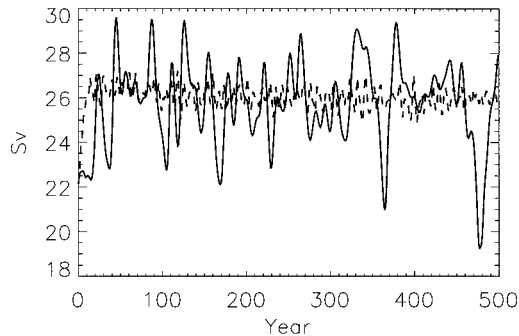


FIG. 22. The overturning index obtained in simulations that examined the sensitivity to the timescale of stochastic forcing. Shown are the time series from a simulation in which the stochastic forcing is low-pass filtered (solid line), and the time series from a simulation in which the stochastic forcing is high-pass filtered (dashed line).

frequency range of the forcing [as suggested by Griffies and Tziperman (1995)]. Figure 22 shows the overturning time series obtained in these simulations. When the applied stochastic freshwater forcing is low-pass filtered, the magnitude and time series of the simulated THC variability is very similar to that obtained in experiment STOCHFW (Table 3). However, when the stochastic forcing is high-pass filtered, the THC variability is greatly reduced and the correlation to experiment STOCHFW is low. This suggests that the THC variability responds linearly and preferentially to the stochastic forcing at interdecadal timescales. This is similar to the results obtained by Delworth and Greatbatch (2000) in the GFDL coupled model and is in agreement with the analysis of Griffies and Tziperman (1995).

Based on the results presented in this section, it appears that the THC variability is linked to modes of the North Atlantic region that are forced by stochastic variability in the freshwater flux. Stochastic forcing at low frequencies is particularly important for driving the THC variability. In the standard simulation, stochastic forcing is provided in the form of ice export from the Arctic. Ice export is an important component of this variability because of the large and highly variable forcing that it supplies to the net freshwater flux into the North Atlantic.

6. Sensitivity to ice–ocean exchange

The above analysis suggests that the stochastic forcing element of Arctic ice export is important for driving THC variability, but that internal Arctic processes have little impact on the timescale of this variability. However, the ice–ocean coupling within the northern North Atlantic appears to play some role in modifying the THC. In this section we examine the importance of the ice–ocean coupling in various sensitivity studies. These include the sensitivity of the coupled system to 1) the ice–ocean freshwater flux and 2) the ice–ocean heat ex-

TABLE 3. Results obtained from experiments that examine the sensitivity of the THC variability to the timescale of the stochastic forcing.

	Low-pass filtered	High-pass filtered
Std dev	1.89 Sv	0.52 Sv
Correlation to STOCHFW	0.89	0.34

change. In these sensitivity runs the feedback mechanisms associated with these different ice–ocean exchange processes are excluded by forcing the model with a constant annual cycle of the relevant ice–ocean flux.

a. Ice–ocean freshwater flux

We have shown that simulated variability in the North Atlantic Ocean is highly dependent on changes in the amount of freshwater input due to ice export and subsequent melting. In this section we examine the sensitivity of the system to ice–ocean freshwater feedbacks by comparing a control simulation to a case where the ice growth/melt component of the freshwater flux is specified to be annually periodic. Ice growth rates are still computed in the model, but they only affect the ice mass balance and do not influence the freshwater coupling between the ice and the ocean. We continue to apply stochastic wind forcing to the ice momentum so the insulating effect of the ice is highly variable. The total impact of the ice–ocean freshwater coupling is examined and compared to the standard simulation. We also examine the influence of the ice–ocean freshwater coupling in a case analogous to experiment STOCHFW. In this simulation annually periodic wind forcing is used and stochastic anomalies are applied to the freshwater flux over the northern North Atlantic. But unlike STOCHFW, the growth/melt component of the freshwater flux is annually periodic.

1) TOTAL FRESHWATER FLUX IMPACT

In addition to its freshwater flux effect, variable ice export causes anomalous insulation of the northern North Atlantic ocean from the relatively cold atmosphere. In some studies (Zhang et al. 1995; Lohmann and Gerdes 1998) the ice insulation has been shown to have a dominant effect on THC stability. In experiment NO_FWFLX1 we examine the sensitivity of the system to ice–ocean freshwater coupling when the ice cover is forced with stochastically varying winds. This sensitivity study was run for 1000 yr from initial conditions obtained from the standard simulation. It allows us to determine the relative importance of the ice-induced freshwater feedbacks compared to the insulating feedbacks for determining THC variability.

When the ice–ocean freshwater feedbacks are suppressed, the variability in the overturning is greatly re-

duced from a standard deviation of 1.9 Sv for the standard simulation to 0.08 Sv for experiment NO_FWFLX1. Because of damping in the system, the highly variable ice export that results in northern North Atlantic ice melt anomalies is necessary to excite the THC variability. Variations in the insulating effects of the ice cover are not sufficient to force this variability.

The variability of the ice cover in the northern North Atlantic is also sensitive to the presence of the ice–ocean freshwater feedbacks. When these feedbacks are suppressed, the variability in the GIN and Labrador sea ice is reduced (Table 2). However, the variability in the ice exported from the Arctic and Baffin Bay into these regions is similar regardless of the presence of these feedbacks. This implies that the variability of the Labrador and GIN sea ice cover partially results from changes in local ice growth mechanisms. Weak variability of the overturning circulation and consequent oceanic heat transport into the ice-covered regions is the most likely culprit for the decreased sea ice variability. It is possible (and as shown below, likely) that the ice cover in the GIN and Labrador seas is not just passively reacting to changes in the overturning, but is also modifying the overturning variability.

2) “NONSTOCHASTIC” FRESHWATER FLUX IMPACT

Much of the influence of ice–ocean freshwater coupling discussed in section 6a(1) is likely due to the stochastic forcing component of the ice melt rates in the northern North Atlantic. This stochastic forcing is necessary to excite THC variability in the presence of damping. There is an additional component to the ice–ocean freshwater coupling that is driven by variable melt rates forced by changes in the SST and resulting variations in ice–ocean heat exchange. In this section, we isolate this second impact by allowing for a variable stochastic freshwater forcing in the ice melt regions. This simulation is identical to experiment STOCHFW, except that the ice–ocean freshwater flux is specified to be annually periodic. It is run for 500 yr from initial conditions obtained from year 500 of experiment STOCHFW. It uses the same stochastic forcing applied for years 500–1000 in experiment STOCHFW. This sensitivity test, which is referred to as experiment NO_FWFLX2, is compared to experiment STOCHFW.

Figure 23 shows the overturning time series and spectrum obtained in the sensitivity test. The ice–ocean freshwater coupling damps the overturning variability, resulting in an overturning index standard deviation of 2.4 Sv for experiment NO_FWFLX2 compared to 1.6 Sv in experiment STOCHFW (for years 500–1000). However, the spectrum of the overturning index shows that the variability at the 20–25-yr timescale is similar regardless of the inclusion of the ice–ocean freshwater flux feedbacks. This implies that this mode of variability may be a damped ocean-only mode that is excited by stochastic freshwater flux anomalies, similar to the mode

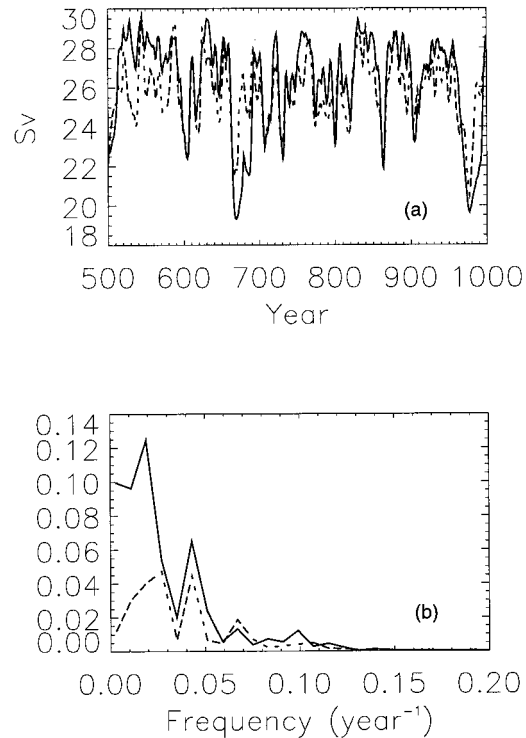


FIG. 23. The (a) time series in Sv and (b) spectrum of the overturning index obtained in experiment NO_FWFLX2. Also shown are the corresponding statistics from experiment STOCHFW (dashed line).

of variability seen in the box model simulations of Griffies and Tziperman (1995). It is also possible that the insulating effects of the ice cover are important for driving this variability.

b. Ice–ocean heat exchange

As discussed above (section 6a), it appears that the variability in the ice–ocean heat exchange has an impact on the variability of the ice cover in the GIN and Labrador Sea regions. To more clearly examine this sensitivity, a simulation is run where the oceanic heat flux to the ice cover is specified to be annually periodic. This simulation, which is referred to as NO_HFLX, effectively removes feedbacks in the system due to the ice–ocean thermal coupling. The insulating and albedo effects of the ice cover are allowed to vary with changes in the ice cover. Thus, the variations in ice cover affect the ocean heat budget, but the ocean heat budget does not cause changes in the ice cover. Atmosphere–ocean and atmosphere–ice heat exchange is not affected in this sensitivity test and occurs as in the standard simulation. This sensitivity test is integrated for 700 yr.

It appears that the presence of the ice–ocean thermal coupling has an impact on the magnitude of the THC variability. When the ice cover receives a constant oceanic heat flux, the standard deviation of the overturning

Standard Deviation Ice Thickness Difference (Standard - NO_HFLX)

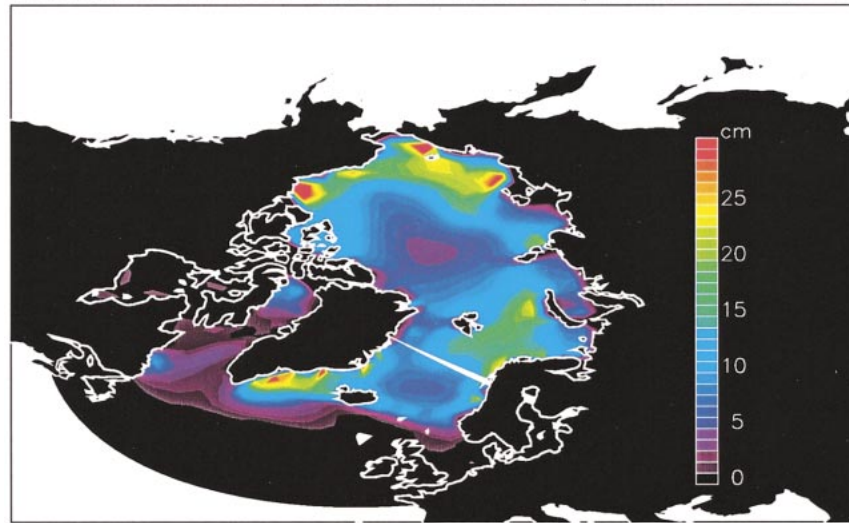


FIG. 24. The difference in the annual-averaged ice thickness standard deviation between the standard run and experiment NO_HFLX.

index is increased by more than 30% (see Table 2) compared to that of the standard simulation. However, the variability in the GIN and Labrador sea ice cover is much reduced, which implies that changes in the local ice growth rates within the GIN and Labrador Seas (forced by changes in the ice–ocean heat flux) are responsible for a large fraction of the variability in the ice cover within these regions.

The enhanced overturning variability seen in experiment NO_HFLX suggests that the ice–ocean heat fluxes (and their resulting changes in the sea ice cover) damp the overturning variability. Thus it appears that in the standard simulation, a low GIN Sea freshwater flux causes an increase in convection in the North Atlantic. Strong convection and increased northward heat transport warms the surface ocean, resulting in lower ice growth rates during the fall. It appears that the reduced brine rejection due to low ice growth rates (Fig. 15) then acts to decrease deep convection and reduces the overturning strength. A similar process is seen in the stochastic freshwater forcing simulation discussed in section 5. This scenario is similar to the ice–ocean feedback loop discussed by Yang and Neelin (1993, 1997). However, unlike Yang and Neelin’s simulations, this feedback has a relatively small effect on the THC variability.

Although variable ice–ocean heat exchange has a large impact on the sea ice variability in the North Atlantic, it has a much smaller impact on ice within the central Arctic Basin. Figure 24 shows the difference in the ice thickness standard deviation between the standard simulation and this sensitivity study. The most notable differences are found along the ice edge in the North Atlantic and within the Arctic shelf regions. The North Atlantic ice edge is affected by the thermohaline

circulation and changes in the ocean surface temperature due to convective and advective changes. The Arctic shelf regions are likely influenced by variability in the absorption of solar radiation in the water column during the summer months. The variability in the remainder of the Northern Hemisphere ice-covered regions appears to be largely driven by the impact of variable winds. However, low-frequency variability in the thickness of ice within the Arctic is reduced. This can be seen in the spectrum of ice export (not shown) which in experiment NO_HFLX is almost entirely driven by ice velocity changes at all timescales. This is in contrast to the standard simulation, in which ice thickness changes played an important role in the low-frequency variability of ice export, resulting in preferred interdecadal timescales.

7. Discussion and conclusions

The export of sea ice from the Arctic into the North Atlantic provides a considerable freshwater forcing for sensitive deep water formation regions. In this study, we examined the impact of simulated variations in Arctic ice motion on the thermohaline circulation and the general characteristics of the North Atlantic climate. A global coupled general circulation ocean–dynamic sea ice–atmospheric energy moisture balance model was used to perform 1000-yr-long simulations. The Arctic ice motion was stochastically forced with wind stress perturbations. These perturbations have the same spatial structure that is present in an empirical orthogonal function analysis of 40 yr of NCEP reanalysis surface pressure fields, but they have stochastic time series.

We find that realistic variability in the simulated Arctic ice export causes fluctuations in the THC that have a standard deviation of approximately 2 Sv (10% of the

simulated mean strength). This variability has enhanced power at interdecadal timescales that are concentrated at a period of approximately 20 yr. It is led by large changes in the temperature and salinity of the northern North Atlantic sea surface, which are caused by changes in the sea ice conditions. These oceanic changes influence the atmospheric state as well, causing changes in air temperature, precipitation, and subsequent river runoff.

The variability in the thermohaline circulation also affects processes within the Arctic Basin. This occurs primarily through the modification of heat transport into the Arctic within the Atlantic layer (the water of Atlantic origin that lies between 200- and 1000-m depth in the Eurasian Basin). The signature of Atlantic layer anomalies can clearly be seen penetrating as far as the Lomonosov ridge. This process is reminiscent of recent observations showing a warming of the Atlantic layer within the Eurasian Basin (Carmack et al. 1995). It highlights the emerging picture of a variable Arctic Ocean. Changes in heat transport affect the growth of sea ice within the Arctic Basin and the thickness of ice that is exported to the North Atlantic. This interaction causes enhanced interdecadal variability to be simulated in the ice export time series.

The sensitivity of the model simulation to the method of stochastic forcing was tested. When the wind forcing of the ice motion was annually periodic but stochastic anomalies were instead applied to the freshwater flux in the northern North Atlantic, the model THC response was similar to that of the standard simulation. The similar behavior suggests that the interdecadal THC variability in the standard simulation is not dependent on the timescales of internal Arctic processes but is excited by the stochastic element of the ice export anomalies. The variability in the ice cover is greatly reduced in the absence of variable wind forcing for all regions except along the northern North Atlantic ice edge. This implies that variable winds are the dominant forcing for Arctic sea ice variability, whereas local ice growth processes are more important for sea ice variability in the northern North Atlantic.

Additional sensitivity tests were performed to determine the impact of ice–ocean coupling on the simulated variability. In particular, we separately examined the influence of the ice–ocean freshwater and thermal coupling. In the standard experiment, the ice–ocean freshwater flux anomalies largely act as a stochastic forcing of the northern North Atlantic Ocean. We find that these variable fluxes are necessary to excite the simulated THC variability. Variations in the insulating effect of the ice cover play a much smaller, secondary role. Due to the model limitations and the fact that very little deep water formation occurs in the GIN Sea region, we may be underestimating the insulating effects of the ice for driving variations in the THC. However, in the Labrador Sea where the convective regions are more accurately simulated, we also obtain that sea ice–induced fresh-

water fluxes are dominant in driving deep water formation variability. While not conclusive, this supports our claim that the sea ice insulating effect is of secondary importance in forcing overturning anomalies.

In additional sensitivity tests, we find that the influence of ice–ocean heat exchange on the northern North Atlantic ice melt rates acts to slightly damp the overturning variability. For example, when the ice growth rates are forced by a constant annual cycle of ocean heat flux, the overturning index standard deviation increases by approximately 30% to 2.4 Sv. In general, the simulated THC variability is reduced due to ice–ocean thermal coupling. It appears that the negative feedback loop that results in this reduced variability is similar to that discussed by Yang and Neelin (1993, 1997) in which changes in northern North Atlantic ice melt rate influence the ocean stability and oceanic heat transport that in turn modifies the ice melt rates. However, in contrast to Yang and Neelin (1993, 1997), this negative feedback plays a relatively small role in modifying the THC variability and is not responsible for the enhanced variability seen at interdecadal timescales. The inclusion of sea ice dynamics, the seasonal cycle, and an interactive atmosphere in the current study are likely responsible for the reduced influence of this feedback.

Although, the ice–ocean heat exchange damps the simulated THC variability, it appears to have little effect on the enhanced interdecadal timescales seen in this variability. This suggests that the variability at these timescales is driven by oceanic processes that are excited by stochastic forcing of the freshwater flux similar to the variability described by Griffies and Tziperman (1995). In the standard simulation, this stochastic forcing is provided by variable ice export and subsequent melting in the northern North Atlantic. The simulated oceanic response to this stochastic forcing is not largely dependent on forcing at frequencies greater than $(10 \text{ yr})^{-1}$.

This study suggests that interdecadal variability is a property of the North Atlantic Ocean system. This variability is driven by stochastic freshwater forcing that in these model simulations is provided by variable wind driven Arctic ice export. The influence of variable winds on the oceanic wind driven circulation and turbulent fluxes has not been addressed here and will possibly modify the simulated variability in the system. This aspect of variable wind forcing on the ice–ocean system will be examined in future work.

An interesting further question raised by this study concerns how the simulated variability seen in the ice–ocean system may in turn feed back onto the atmospheric circulation. These potential feedbacks may help explain observed variations in, for example, the North Atlantic oscillation. The model used here is inadequate to address this issue due to the simplicity of the atmospheric system. Future work is needed to consider changes in the atmospheric circulation that are forced by sea ice and ocean conditions.

Acknowledgments. We would like to thank two anonymous reviewers for helpful comments. This research was supported by International Arctic Research Center, NSERC, Atmospheric Environment Service, Canadian Institute for Climate Studies, and IBM SUR research grants. NCEP Reanalysis data was provided by the NOAA CIRES Climate Diagnostics Center, Boulder, Colorado, from their Web site at <http://www.cdc.noaa.gov>.

REFERENCES

- Aagaard, K., and E. C. Carmack, 1989: The role of sea ice and other fresh water in the Arctic circulation. *J. Geophys. Res.*, **94**, 14 485–14 498.
- Beckmann, A., and R. Doescher, 1997: A method for improved representation of dense water spreading over topography in geopotential-coordinate models. *J. Phys. Oceanogr.*, **27**, 581–591.
- Bourke, R. H., and R. P. Garret, 1987: Sea ice thickness distribution in the Arctic Ocean. *Cold Reg. Sci. Technol.*, **13**, 259–280.
- Broeker, W. S., D. M. Petet, and D. Rind, 1985: Does the ocean-atmosphere system have more than one stable mode of operation? *Nature*, **315**, 21–26.
- Bryan, K., and L. Lewis, 1979: A water mass model of the world ocean. *J. Geophys. Res.*, **84**, 2503–2517.
- Capotondi, A., and W. R. Holland, 1997: Decadal variability in an idealized ocean model and its sensitivity to surface boundary conditions. *J. Phys. Oceanogr.*, **27**, 1072–1093.
- , and —, 1998: Thermohaline circulation variability in the NCAR Climate System Model (CSM). NCAR Tech. Note TN-445 + STR, 25 pp.
- Carmack, E. C., R. W. Macdonald, R. G. Perkin, F. A. McLaughlin, and R. J. Pearson, 1995: Evidence for warming of Atlantic water in the southern Canadian Basin of the Arctic Ocean: Results from the Larsen-93 expedition. *Geophys. Res. Lett.*, **22**, 1061–1064.
- Delworth, T. L., and R. J. Greatbatch, 2000: Multidecadal thermohaline circulation variability driven by atmospheric surface flux forcing. *J. Climate*, **13**, 1481–1495.
- , S. Manabe, and R. J. Stouffer, 1993: Interdecadal variations of the thermohaline circulation in a coupled ocean-atmosphere model. *J. Climate*, **6**, 1993–2011.
- , —, and —, 1997: Multidecadal climate variability in the Greenland Sea and surrounding regions: A coupled model simulation. *Geophys. Res. Lett.*, **24**, 257–260.
- Deser, C., and M. L. Blackmon, 1993: Surface climate variations over the North Atlantic Ocean during winter: 1900–1989. *J. Climate*, **6**, 1743–1753.
- Dickson, R. R., J. Lazier, J. Meincke, P. Rhines, and J. Swift, 1996: Long term coordinated changes in the convective activity of the North Atlantic. *Progress in Oceanography*, Vol. 38, Pergamon, 205–293.
- , J. Meincke, S. A. Malmberg, and A. J. Lee, 1988: The “Great Salinity Anomaly” in the northern North Atlantic 1968–1982. *Progress in Oceanography*, Vol. 20, Pergamon, 103–151.
- Duffy, P., M. Eby, and A. Weaver, 1999: Effects of sinking of salt rejected during formation of sea ice on results of a global ocean-atmosphere-sea ice climate model. *Geophys. Res. Lett.*, **26**, 1739–1742.
- Eby, M., and G. Holloway, 1994: Grid transformation for incorporating the Arctic in a global ocean model. *Climate Dyn.*, **10**, 241–247.
- Fanning, A. F., and A. J. Weaver, 1996: An atmospheric energy-moisture balance model: Climatology, interpentadal climate change, and coupling to an ocean general circulation model. *J. Geophys. Res.*, **101**, 15 111–15 128.
- Flato, G. M., and W. D. Hibler, 1995: Ridging and strength in modeling the thickness distribution of Arctic sea ice. *J. Geophys. Res.*, **100**, 18 611–18 626.
- Gent, P. R., and J. McWilliams, 1990: Isopycnal mixing in ocean circulation models. *J. Phys. Oceanogr.*, **20**, 150–155.
- Graves, C. E., W.-H. Lee, and G. R. North, 1993: New parameterizations and sensitivities for simple climate models. *J. Geophys. Res.*, **98**, 5025–5036.
- Griffies, S., and E. Tziperman, 1995: A linear thermohaline oscillator driven by stochastic atmospheric forcing. *J. Climate*, **8**, 2440–2453.
- , and K. Bryan, 1997: A predictability study of simulated North Atlantic multidecadal variability. *Climate Dyn.*, **13**, 459–487.
- Häkkinen, S., 1993: An Arctic source for the Great Salinity Anomaly: A simulation of the Arctic ice-ocean system for 1955–1975. *J. Geophys. Res.*, **98**, 16 397–16 410.
- Hasumi, H., and N. Sugimoto, 1995: Haline circulation induced by formation and melting of sea ice. *J. Geophys. Res.*, **100**, 20 613–20 625.
- Hibler, W. D., 1980: Modeling a variable thickness ice cover. *Mon. Wea. Rev.*, **108**, 1943–1973.
- Holland, M. M., J. A. Curry, and J. L. Schramm, 1997: Modeling the thermodynamics of a distribution of sea ice thicknesses. Part II: Sea ice/ocean interactions. *J. Geophys. Res.*, **102**, 23 093–23 107.
- Hunke, E. C., and J. K. Dukowicz, 1997: An elastic-viscous-plastic model for sea ice dynamics. *J. Phys. Oceanogr.*, **27**, 1849–1867.
- Hurrell, J. W., 1995: Decadal trends in the North Atlantic Oscillation: Regional temperatures and precipitation. *Science*, **269**, 676–679.
- Kushnir, Y., 1994: Northern hemisphere sea surface temperature and associated atmospheric conditions. *J. Climate*, **7**, 141–157.
- Kwok, R., and D. Rothrock, 1999: Variability of Fram Strait ice flux and North Atlantic Oscillation. *J. Geophys. Res.*, **104**, 5177–5189.
- Lazier, J. R. N., 1980: Oceanographic conditions at Ocean Weather Ship Bravo, 1964–1974. *Atmos.–Ocean*, **18**, 227–238.
- Levitus, S., 1989: Interpentadal variability of temperature and salinity at intermediate depths of the North Atlantic Ocean, 1970–1974 versus 1955–1959. *J. Geophys. Res.*, **94**, 6091–6131.
- Lohmann, G., and R. Gerdes, 1998: Sea ice effects on the sensitivity of the thermohaline circulation. *J. Climate*, **11**, 2789–2803.
- Mauritzen, C., and S. Häkkinen, 1997: Influence of sea ice on the thermohaline circulation in the Arctic–North Atlantic Ocean. *Geophys. Res. Lett.*, **24**, 3257–3260.
- Maykut, G. A., 1982: Large-scale heat exchange and ice production in the central Arctic. *J. Geophys. Res.*, **87**, 7971–7984.
- Mikolajewicz, U., and E. Maier-Reimer, 1990: Internal secular variability in an ocean general circulation model. *Climate Dyn.*, **4**, 145–156.
- Pacanowski, R., 1995: MOM 2 Documentation, user’s guide and reference manual. GFDL Ocean Group Tech. Rep. 3, GFDL, Princeton, NJ, 232 pp. [Available online at <http://www.gfdl.gov/~smg/mom/mom.html>.]
- Semtner, A. J., 1976: A model for the thermodynamic growth of sea ice in numerical investigations of climate. *J. Phys. Oceanogr.*, **6**, 379–389.
- Serreze, M. C., J. A. Maslanik, R. G. Barry, and T. Demaria, 1992: Winter atmospheric circulation in the Arctic Basin and possible relationships to the Great Salinity Anomaly in the northern North Atlantic. *Geophys. Res. Lett.*, **19**, 293–296.
- Stommel, H., 1961: Thermohaline convection with two stable regimes of flow. *Tellus*, **13**, 224–230.
- Taylor, K., G. Lamorey, G. Doyle, R. Alley, P. Grootes, P. Mayewski, J. White, and L. Barlow, 1993: The “flickering switch” of late Pleistocene climate change. *Nature*, **361**, 432–435.
- Timmermann, A., A. Latif, R. Voss, and A. Grotzner, 1998: Northern hemisphere interdecadal variability: A coupled air–sea model. *J. Climate*, **11**, 1906–1931.
- Vinje, T., N. Nordlund, and Å. Kvambekk, 1998: Monitoring ice thickness in Fram Strait. *J. Geophys. Res.*, **103**, 10 437–10 449.
- Walsh, J. E., and W. L. Chapman, 1990: Arctic contribution to upper-ocean variability in the North Atlantic. *J. Climate*, **3**, 1462–1473.
- Weaver, A. J., E. Sarachik, and J. Marotzke, 1991: Freshwater flux

- forcing of decadal and interdecadal oceanic variability. *Nature*, **353**, 836–838.
- , C. M. Bitz, A. F. Fanning, and M. M. Holland, 1999: Thermohaline circulation: High latitude phenomena and the difference between the Pacific and Atlantic. *Ann. Rev. Earth Planet. Sci.*, **27**, 231–285.
- Weisse, R., U. Mikolajewicz, and E. Maier-Reimer, 1994: Decadal variability of the North Atlantic in an ocean general circulation model. *J. Geophys. Res.*, **99**, 12 411–12 421.
- Winton, M., and E. Sarachik, 1993: Thermohaline oscillations induced by strong steady salinity forcing of ocean general circulation models. *J. Phys. Oceanogr.*, **23**, 1389–1410.
- Yang, J., and J. D. Neelin, 1993: Sea ice interactions with the thermohaline circulation. *Geophys. Res. Lett.*, **20**, 217–220.
- , and ———, 1997: Decadal variability in coupled sea-ice-thermohaline circulation systems. *J. Climate*, **10**, 3059–3076.
- Zhang, S., C. A. Lin, and R. J. Greatbatch, 1995: A decadal oscillation due to the coupling between an ocean circulation model and a thermodynamic sea-ice model. *J. Mar. Res.*, **53**, 79–106.